ACOUSTICS 2017 PERTH
SOUND, SCIENCE AND SOCIETY

A measurement campaign for railway-induced vibrations in a building

Kirsty Kuo (1), Kristof Maes (1), Matthias Germonpré (1), Geert Lombaert (1) and Geert Degrande (1)

(1) Department of Civil Engineering, KU Leuven, Leuven, Belgium

ABSTRACT

In October 2016, an extensive field measurement campaign was conducted at a site in Belgium where a three-storey building with a basement is located 33m from a railway line that is used by both freight and passenger trains. Over a period of eleven days, the dynamic response in the free field and the building was measured simultaneously, resulting in a database of over 500 train passages. Nine measurement locations were used in the free field, and sixteen measurement locations were spread across the four floors of the building. In a second set of measurements, transfer functions were obtained using excitations from an impact hammer at a series of 17 sleeper locations over a total distance of 196 m. The vibration levels within the building are, on the whole, smaller than those measured directly outside the building. There is no clear trend of attenuation with floor height, and although it would generally be expected that mid-span locations would have higher vibration levels than near-column locations, this study shows that this is not always the case.

1 INTRODUCTION

Due to the demand for mass transit in urban areas, railways and buildings are being situated in ever-closer proximity. The propagation of ground-borne vibrations, occurring in the 1-80 Hz range, into these buildings can be disturbing to residents and disruptive to sensitive manufacturing processes. Vibration level limits exist to minimise disturbance from railway-induced vibrations, and accurate prediction models are needed to ensure that these legal limits are met.

Amongst vibration consultants, empirical formulae that account for vibration attenuation from the train and track, through the soil and into the foundation and building are a popular and easy-to-implement approach. Examples of empirical methods include the procedures developed by the Federal Railroad Administration (FRA) and the Federal Transit Administration (FTA) of the U.S. Department of Transportation (Hanson, Towers, and Meister 2006, 2005), the Swiss Federal Railways (SBB) (Kuppelwieser and Ziegler 1996), Madshus et al. (Madshus, Bessason, and Hårvik 1996), and Hood et al. (Hood et al. 1996). Following the guidance of the ISO 14837-1 standard (International Organization for Standardization 2005), the procedures developed by the FRA and FTA involve three different levels of assessment: a screening procedure, a general environmental assessment, and a detailed vibration analysis. The first two levels are used to screen for vibration sensitive sites. The third level uses field measurements of excitation forces and transmission paths to estimate the ground response, to which adjustment factors are applied for calculation of the building response (Bovey 1983; Nelson and Saurenman 1987). The advantage of this method is that it avoids the need for extensive soil characterisation tests by directly measuring the vibration transmission through the soil (Hanson, Towers, and Meister 2006).

In this paper, we present an extensive measurement campaign that was carried out with the aim of calculating the excitation forces, transmission paths and building response as per the FRA procedure, introduced in section 2. In section 3 the layout of the site is described and section 4 details the equipment used. The data processing procedure is presented in section 5. The results of the study are presented and discussed in section 6, which is followed by the conclusions in section 7.

2 FRA PROCEDURE

The empirical procedure proposed by the FRA (Hanson, Towers, and Meister 2006) is expressed as:

$$\mathrm{L_v}(\mathbf{x_b}) = \mathrm{L_F}(\mathbf{X}, \mathbf{x_1}) + \mathrm{TM_L}(\mathbf{X}, \mathbf{x_1}) + \mathrm{C_b}(\mathbf{x_1}, \mathbf{x_b}) \tag{1}$$

where $\mathbf{X}$ is a vector that collects all of the source points, located on the rail heads. The receiver points $\mathbf{x}_1$ and $\mathbf{x}_\mathrm{b}$ are located at some point on the ground surface, and at some point inside the building, respectively. The term $\mathrm{L_v}(\mathbf{x_b})$ is the vibration velocity level at the receiver point $\mathbf{x}_\mathrm{b}$ in the building, and is measured in decibels at one-third octave band intervals.

The excitation force, represented by the equivalent force density level $\mathrm{L_F}(\mathbf{X},\mathbf{x}_1)$, is calculated as the difference between the measured vibration velocity level at some point on the ground surface $\mathbf{x}_1$ and the line source transfer mobility level:

$$\mathrm{L_F}(\mathbf{X},\mathbf{x}_1) = \mathrm{L_v}(\mathbf{x}_1) - \mathrm{TM_L}(\mathbf{X},\mathbf{x}_1) \tag{2}$$

This excitation force term represents the equivalent fixed line source that results in the same vibration velocity level as the train passage. The force density level depends on both the actual force generated at the wheel/rail interface and the dynamic characteristics of the transit structure (that is, the tunnel or ballast and the soil).

The vibration propagation from the track, through the soil to the receiver point on the soil surface is contained within the line source transfer mobility term $\mathrm{TM_L}(\mathbf{X},\mathbf{x}_1)$. This involves the superposition of point source transfer mobility levels $\mathrm{TM_P}(\mathbf{X}_k,\mathbf{x}_1)$ for a series of n equidistant source points with spacing h:

$$\mathrm{TM_L}(\mathbf{X},\mathbf{x}_1) = 10\log_{10}\left[h\sum_{k=1}^{n} 10^{\frac{\mathrm{TM_P}(\mathbf{X}_k,\mathbf{x}_1)}{10}}\right] \tag{3}$$

The dynamic soil-structure interaction (SSI) between a building and a railway is then characterised using a coupling loss term $\mathrm{C_b}(\mathbf{x}_1,\mathbf{x}_\mathrm{b})$ that accounts for ground-building foundation interaction and amplification or attenuation of vibration amplitudes as vibration propagates through buildings. The FRA approach defines the coupling loss term using three adjustment factors that are applied to the free field vibration velocity level: (a) those that represent the change in the incident ground-surface vibration due to the presence of the building foundation, (b) the attenuation of vibration as it travels from foundation to the upward floors, assumed at a rate of 1 to 2 dB per floor, and (c) amplification of approximately 6 dB in the frequency range of the fundamental floor resonances (15-20 Hz for wood-frame, 20-30 Hz for reinforced concrete slabs). For (a), zero correction is applied when estimating basement floor vibration or vibration of at-grade slabs, and frequency-dependent attenuation ranging from 0-15 dB is prescribed for masonry buildings on piles and spread footings. An alternative method of defining the coupling loss (Kuo, Lombaert, and Degrande 2017) uses the difference in vibration velocity level, due to a train passage, at some point in the building $\mathrm{L_v}(\mathbf{x}_\mathrm{b})$, and at some point on the ground surface $\mathrm{L_v}(\mathbf{x}_1)$. This is expressed as:

$$\mathrm{C_b}(\mathbf{x}_1,\mathbf{x}_\mathrm{b}) = \mathrm{L_v}(\mathbf{x}_\mathrm{b}) - \mathrm{L_v}(\mathbf{x}_1) \tag{4}$$

3 SITE OVERVIEW

An extensive field measurement campaign was carried out in October 2016 at a site located on the railway line L1390 between Leuven and Ottignies, Belgium. The railway line consists of two classical ballasted tracks with continuously welded UIC 60 rails that are supported every 0.60 m by resilient studded rubber pads on a prestressed monoblock concrete sleeper. Both freight trains and passenger trains of type Desiro ML AM08, built by Siemens, operate on the line.

Located at a distance of 33 m from the nearside track, 'Block D' is a three-storey building with a below-ground basement, and is currently being used for administrative services. It is shown in figure 1. The building is connected to two other nearby buildings through corridors in the basement and on the ground floor. The construction of the Block D building is reinforced concrete and masonry with internal partition walls. Each floor has an area of 350 m^2. There are two nearby roads situated at approximately 25 m and 55 m from the building, and the nearby KU Leuven Data Centre (30 m away) contains large fans that have been previously observed as harmonic sources of vibration.

4 MEASUREMENT SET-UP

During the measurement campaign, the dynamic response on the sleeper, in the free field and in the building was measured simultaneously over a period of seven days, which resulted in a database of over 500 freight and passenger train passages. Ten PCB shock accelerometers were installed on ten consecutive sleepers and are denoted by TS-$\alpha\alpha$-z, where $\alpha\alpha$ denotes the number of the sleeper. The free field vibration measurements were recorded using eighteen high sensitivity uniaxial seismic accelerometers (PCB393 series) and two GeoSIG GMSplus units, measuring accelerations along three measurement lines located perpendicular to the track, as shown in figure 2. On line 1, both the vertical (z) and horizontal ($-x$) accelerations were measured. On line 2, only the vertical (z) accelerations were measured. On line 3, the accelerations in the vertical (z) and the two orthogonal horizontal directions ($-x$ and $-y$) were measured. The dynamic response of the building was measured at four locations on each level of the building (basement, ground floor, first floor and second floor) using twelve GeoSIG GMS-18 units and three GeoSIG GMSplus units. Figure 3 shows the four measurement locations on the first floor

Figure 1: The Block D building is a three-storey building with below-ground basement, located approximately 30 m from the railway track.

of Block D; these measurement locations were mirrored for each floor. The sensor designation used here has two numbers to denote the floor level (91, 00, 01, 02 for basement through to second floor), followed by three numbers to denote the location within the floor space, then followed by the measurement direction(s) (x, y, z). The Nyquist frequency for the PCB accelerometers is 500 Hz, and the Nyquist frequency for the GeoSIGs is 100 Hz. The two measurement systems were time-synchronised using simultaneous acquisition of a signal on the second floor of the building.

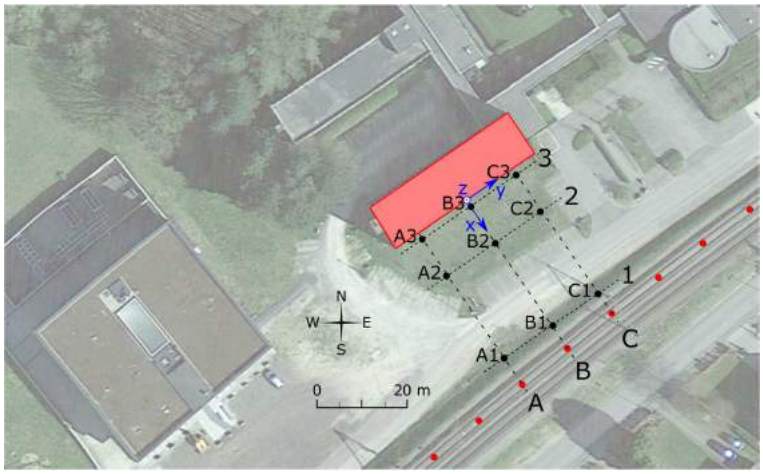

Figure 2: Free field measurement locations (black dots). The measurement lines A, B, and C correspond to $y = -12$ m, $y = 0$ m and $y = 12$ m, respectively. The measurement lines 1, 2, and 3 correspond to $x = 32$ m, $x = 12$ m, and $x = 1$ m, respectively. Eight of the seventeen hammer impact locations are also shown (red dots).

5 DATA PROCESSING

5.1 Train passages

The train passage events are isolated using a trigger on a high sensitivity accelerometer installed on a sleeper to obtain an event window of 131 s. A 5th order Butterworth filter is applied to smooth the noise in the first 1% and final 1% of the time window. A third order Chebyshev filter with high-pass frequency 4 Hz, low-pass frequency of 449 Hz for PXI data and 99 Hz for GMS data, and a ripple of 0.1 dB is applied to avoid drifting of the signal. The velocity is then computed by integration of the acceleration using a trapezium rule.

The German DIN standard (Deutsches Institut für Normung 1995) is used to identify the stationary part of the velocity response for each event, on each channel. This standard defines three time intervals: T_1, T_2, and T_3. Time period T_1 is the interval of 4 s around the maximum running RMS value $v^k_{i,\mathrm{RMS}}(t)$ during the first 14 s of the train passage. Within time period T_1, the maximum velocity $v^k_{i,\max} = \max[v^k_i(t)]$ is computed. Time period T_2 is determined

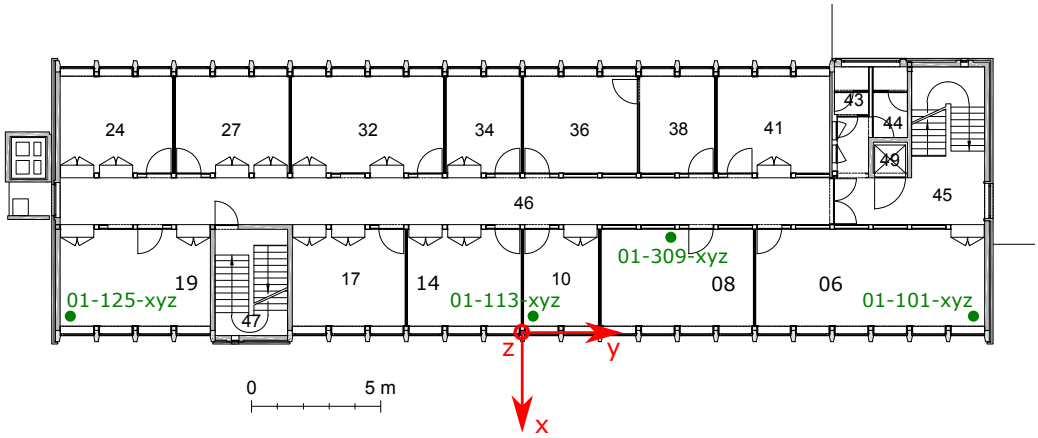

Figure 3: Measurement locations at the first floor of Block D.

as the smallest extension of T_1 such that the velocity $v_i^k(t)$ does not exceed a value $v_{i,\max}^k/4$ within 0.5 s just before and just after T_2. If necessary, the interval T_1 is adjusted to make it a subset of T_2. Finally, the noise amplitude is defined as the mean value of $v_{i,\mathrm{RMS}}^k(t)$ in the measured time interval outside the time period T_2. The time period T_3 is determined as the largest extension of T_2 in which $v_{i,\mathrm{RMS}}^k(t)$ exceeds the noise amplitude.

The time period T_2 was used for this analysis, as it provides a window that encompasses the full length of these trains as observed by the sensors in the free field and the building. The narrow band frequency content of the signal within this time period is used to calculate the RMS value of the velocity $v_{\mathrm{RMS}m}$ in the mth one-third octave band, which can then be used to obtain the vibration velocity level as per:

$$\mathrm{L_v} \quad = \quad 20\log_{10}[v_{\mathrm{RMS}m}] - \mathrm{L_{v0}} \tag{5}$$

where $\mathrm{L_{v0}} = 20\log_{10}[v_0]$ is the reference level calculated using a reference velocity of $v_0 = 10^{-8}$m/s.

To illustrate this process, the acceleration and velocity time histories, running RMS value, frequency content and RMS velocity values for a passenger train with three wagons as observed by a sensor located on the ground floor of the building is shown in figure 4. The three time periods T_1, T_2, and T_3 are indicated on the velocity time history using different colours. The passage of the bogies is not clearly distinguishable within the time history. As the velocity time history and the running RMS values show a response that lacks peaks, there is not as great a difference between the vibration velocities calculated using the three different DIN time periods.

The train type and direction of travel were identified using video footage. The train speed was estimated using the maximum value of the cross-correlation of the acceleration response for a pair of sleeper sensors, as the measured response at these two locations should be similar except for a time delay determined by the speed of the train and the distance between the sensors. As there are ten sleeper sensors, five estimates of the train speed were obtained, and after removing outliers according to Chauvenet's criterion, the speed estimates were averaged.

5.2 Transfer functions

In a second set of measurements, transfer functions were obtained using excitations from an impact hammer with a mass of 5.5 kg and a soft tip equipped with a force sensor (PCB 086D50). Hammer impacts were applied to sleepers located every 12 m along the track, over a total distance of 196 m. The response in the free field and in the building is obtained by integrating the acceleration time signals to obtain the velocity response, and computing the mobility between each source and receiver using the force history. Then the average transfer function is calculated using over 100 hammer impacts at each impact location.

6 RESULTS

6.1 Vibration velocity level

Of the recorded train passages, 117 are three-carriage passenger trains of type Desiro ML AM08, built by Siemens, travelling towards Leuven on the nearside track in a speed range of 77-100 km/h. The measured vertical vibration velocity in one-third octave bands during one of these passages at various distances from the track and at various floors in the building is shown in figure 5. As the distance between the surface measurement point

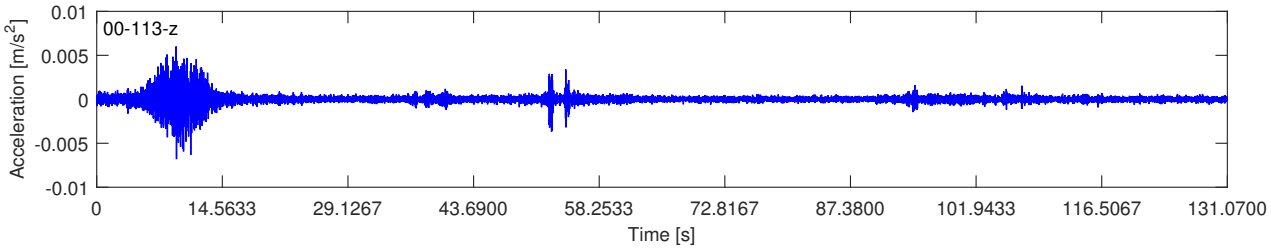

(a)

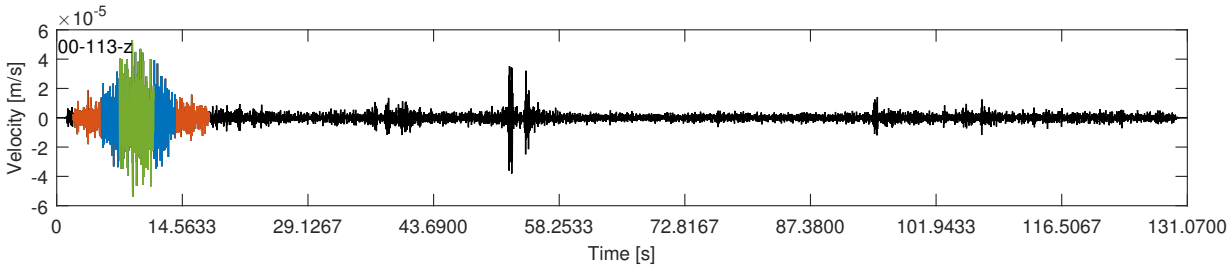

(b)

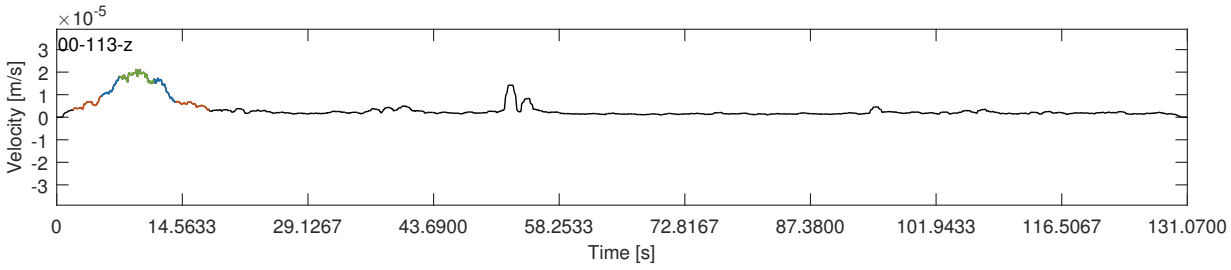

(c)

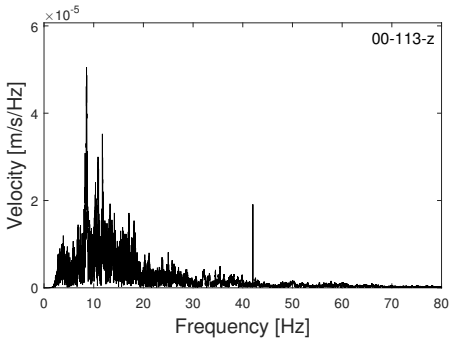

(d)

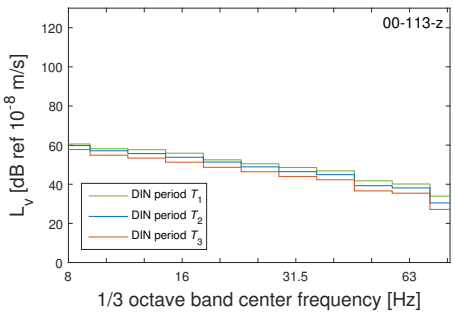

(e)

Figure 4: A passenger train with three wagons observed by the ground-floor building sensor 00-113-z: (a) acceleration time history; (b) velocity time history; (c) running RMS value; (d) frequency content; (e) one-third octave band RMS level.

and the railway increases, the vibration level attenuates with distance from the track due to a combined effect of geometrical spreading and material damping in the soil. The effect of changing the height of the measurement point location within the building, as seen in figure 5(b), is more pronounced at frequencies greater than 25 Hz, but there is no clear trend of vibration attenuation with floor height. This corresponds with the findings of Xia et al. (Xia et al. 2009), who observed fluctuating vertical velocity levels with floor elevation, but runs counter to the FRA recommendation of an adjustment factor of 1-2 dB attenuation per floor. The vibration levels within the building are, on the whole, smaller than those measured directly outside the building. This again concurs with the general trend observed by Xia et al. (Xia et al. 2009). (Note that the 10 dB difference between inside and outside levels quoted by Xia et al. is not directly comparable to the results presented here, as Xia et al. use the maximum of the running RMS velocity calculated using a 1 s interval whereas our results use the RMS velocity values calculated over period T_2 as per the DIN standard.) The FRA approach proposes zero correction when estimating basement floor vibration, which is not supported by these results.

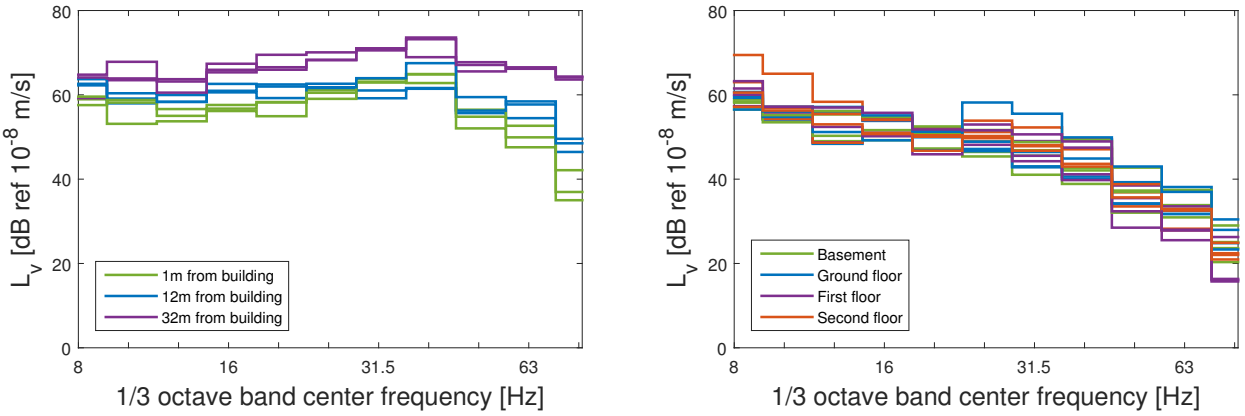

(a) (b)

Figure 5: Vertical vibration velocity levels for a passenger train travelling towards Leuven at 90 km/h measured (a) in the free field along three measurement lines; and (b) in Block D at four measurement locations within each storey.

By collating the data from the 117 train passages, average vibration velocity levels can be determined. Figure 6 shows the average vertical vibration velocity in one-third octave bands at various distances from the track and at various floors in the building. The same trends that were observed for the single passage in figure 5 are also observed in the averaged vibration velocities. The 95% confidence intervals (CIs) for the vibration velocity levels are displayed as shaded regions on these plots and are of the order of 1-3 dB over the entire frequency range, which is notably narrow when compared to the CIs obtained using train passage measurements at another site (Kuo, Lombaert, and Degrande 2016).

6.2 Line source transfer mobility

Figure 7 shows point source transfer mobilities in the free field and in the building using over 100 hammer impacts on the sleeper located at $y = 0$. Non-uniform decay with increasing distance from the track is again seen in the free field. As the attenuation is stronger for higher frequencies, the peak of the frequency content is shifted towards lower frequencies. There appears to be some trend of vibration amplification with floor height in the frequency range of 8-32 Hz.

Figure 8 shows the line source transfer mobilities in the free field and in the building, determined as the summation of the seventeen point source transfer mobilities according to equation 3. Apart from the increase in magnitude due to the summation of multiple point source transfer mobilities, the line source transfer mobilities bear a strong similarity to the point source transfer mobilities shown in figure 7.

6.3 Force density

Figure 9 shows the force density terms calculated using the average vibration velocities shown in figure 6 and the line source transfer mobilities shown in figure 8. It can be seen from these plots that the magnitude and the frequency-dependence of the force density is similar regardless of which receiver points are used. There exists some scatter, particularly at frequencies greater than 35 Hz, but this scatter does not show a strong dependance on distance from the building nor floor elevation. Assuming equivalent force terms therefore appears to be reasonable for this site.

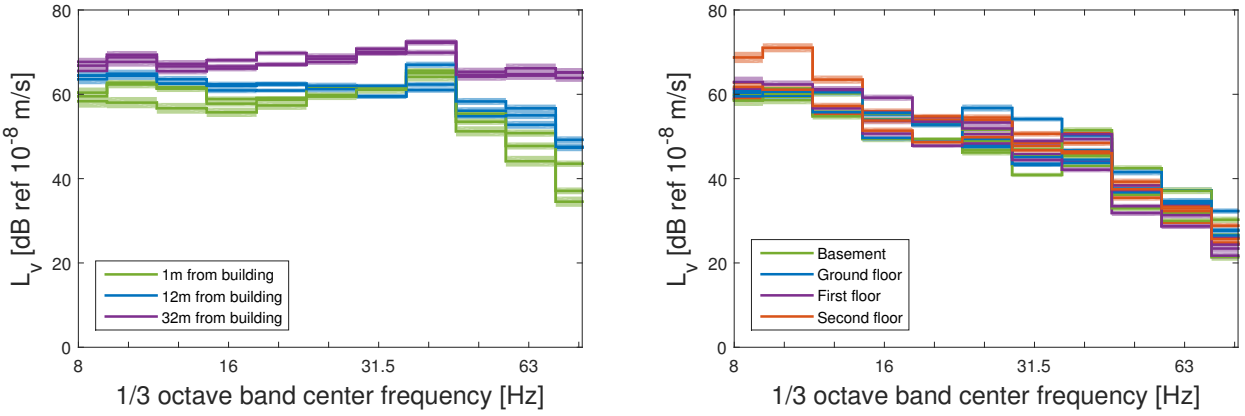

(a) (b)

Figure 6: Average vertical vibration velocity levels determined using 117 passenger train passages (77-100 km/h) measured (a) in the free field along three measurement lines; and (b) in Block D at four measurement locations within each storey. Shaded areas indicate the 95% confidence intervals.

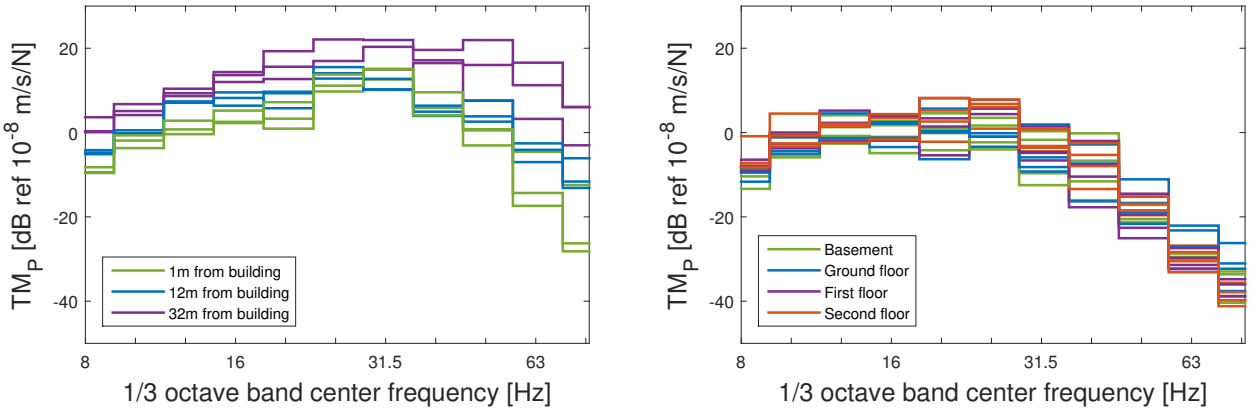

(a) (b)

Figure 7: Point source transfer mobilities determined using more than 100 hammer excitations on the sleeper at $y = 0$ and measured (a) in the free field along three measurement lines; and (b) in Block D at four measurement locations within each storey.

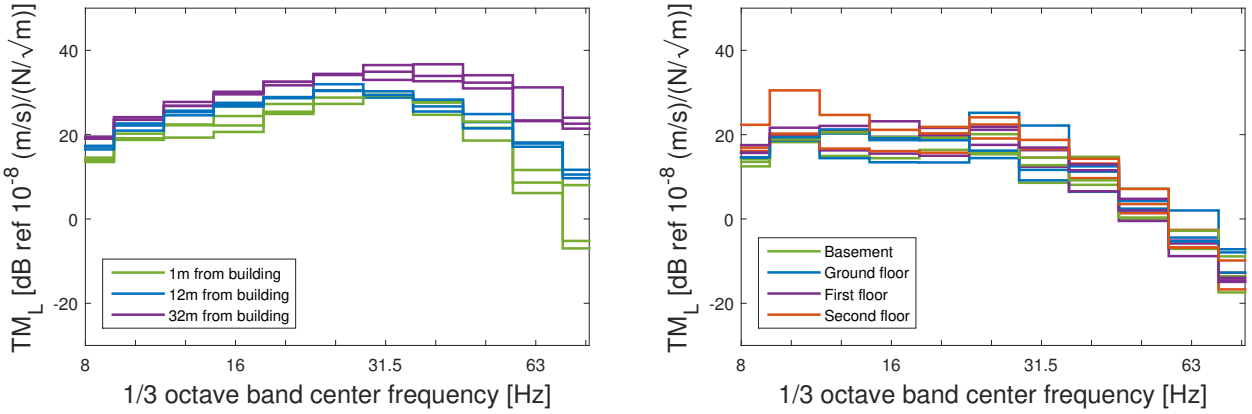

(a) (b)

Figure 8: Line source transfer mobilities determined using more than 100 hammer excitations on the sleeper at each of seventeen source locations and measured (a) in the free field along three measurement lines; and (b) in Block D at four measurement locations within each storey.

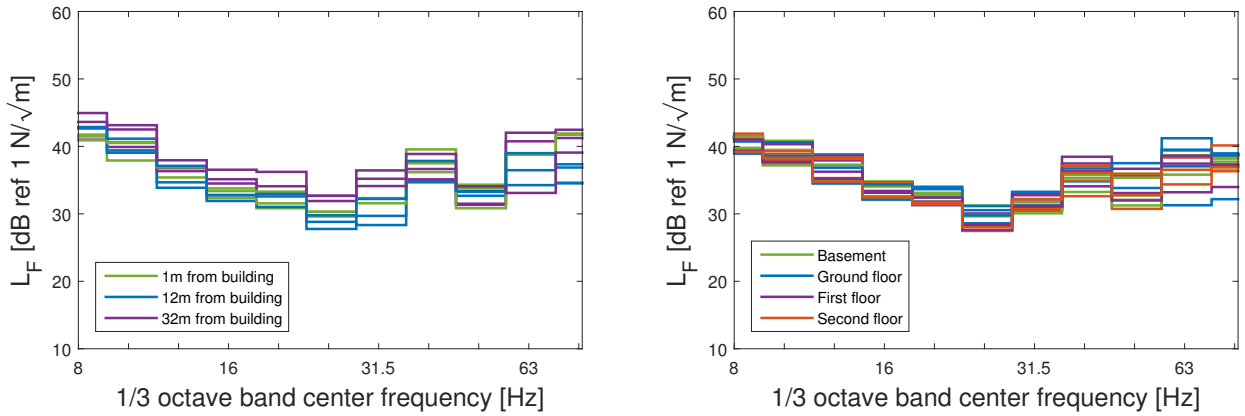

(a) (b)

Figure 9: Force density calculated using using average vibration velocities resulting from 117 passenger train passages (77-100 km/h) and line source transfer mobilities determined using more than 100 hammer excitations on the sleeper at each of seventeen source locations. Sensors are located (a) in the free field along three measurement lines; and (b) in Block D at four measurement locations within each storey.

6.4 Coupling loss

Figure 10 shows the coupling loss calculated using equation (4), where $\mathbf{x}_b$ is located at each of the four points within the floor space, and on each floor, and the location of $\mathbf{x}_1$ is 1 m from the building along each of the three measurement lines A, B and C. The 95% confidence intervals are shown as shaded regions on these plots and are remarkably narrow across the entire frequency range.

Figures 10(a)-(c) show the coupling loss values for building receivers that are located near structural columns, and below the frequency of approximately 25 Hz there is very little difference between the coupling loss values at various floors for two of these receivers. For sensor position XX-125-z, the trend of increasing floor vibration with increasing floor elevation is observed. Figure 10(d) shows the coupling loss value for a building receiver that is located mid-span, and it can be seen that at less than 11 Hz there is a large response on the second floor, and, to a lesser extent, on the first floor. Further vibration measurements inside the building and finite element analysis confirmed that this is due to a dominant, fundamental building mode that involves some coupling between the first and second floors. Although it would generally be expected that the mid-span location would have higher vibration levels than the near-column locations, this study shows that this is not always the case.

The greatest variation between coupling loss values at various floors occurs at frequencies greater than 25 Hz. Comparing the plots in figure 10 along a column (i.e. from top to bottom) gives an indication of how the coupling loss varies with sensor location within the building, and comparing the plots along a row (i.e. from left to right) indicates how the coupling loss varies with sensor location within the free field. In general, there is greater similarity along the rows than the columns, which indicates that the coupling loss is more sensitive to the location of the sensor in the building than in the free field. The main diagonal of figures 10(a) to (c) shows the coupling loss values calculated using the free field sensor that is located closest to the respective building sensors. Due to the symmetry of the measurement setup about the centre of the building, there is the same distance separating sensors XX-125-z/FF-A3-z and sensors XX-101-z/FF-C3-z and the coupling loss values at the ground floor bear a strong resemblance. There is a smaller distance separating sensors XX-113-z/FF-B3-z. The level of variation between the four sensor locations within each floor, and between the three free field locations, can be 10 dB or higher, which represents a significant level of coupling loss dependence on locations $\mathbf{x}_b$ and $\mathbf{x}_1$.

7 CONCLUSIONS

A vibration measurement campaign was carried out in October 2016 at the Block D building that is located near to a frequently used railway. Accelerations were recorded on the track, in the free field and in the building as a result of train passages and hammer impacts on the sleepers. The vibration levels attenuate with distance from the track, and the presence of the building generates further vibration attenuation. Within the building, there are fluctuating vertical velocity levels with floor elevation. The force density terms are similar regardless of whether they are calculated with the receiver sensor in the building or the free field, which indicates that the source term is decoupled from the receiver. The coupling loss terms show a strong dependence on frequency and are more sensitive to the location of the sensor in the building than the location of the sensor in the free field.

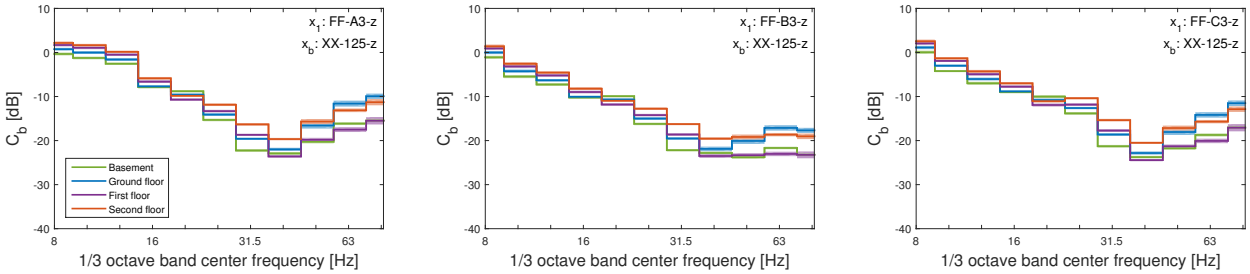

(a)

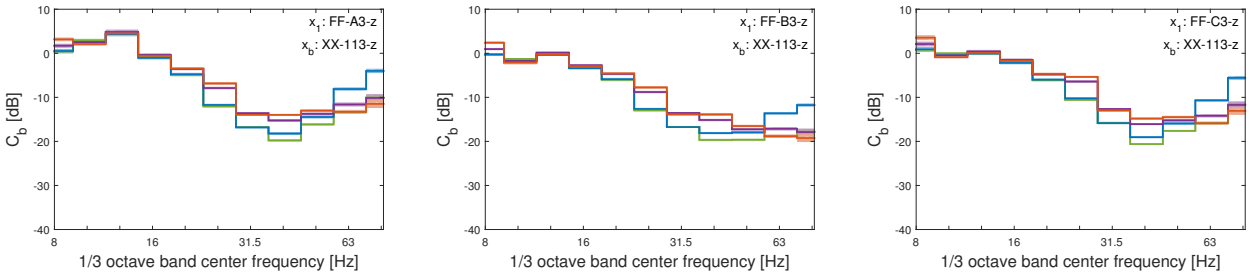

(b)

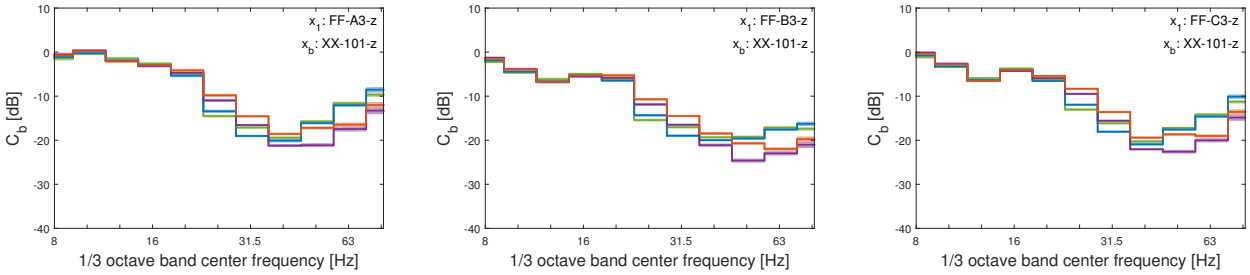

(c)

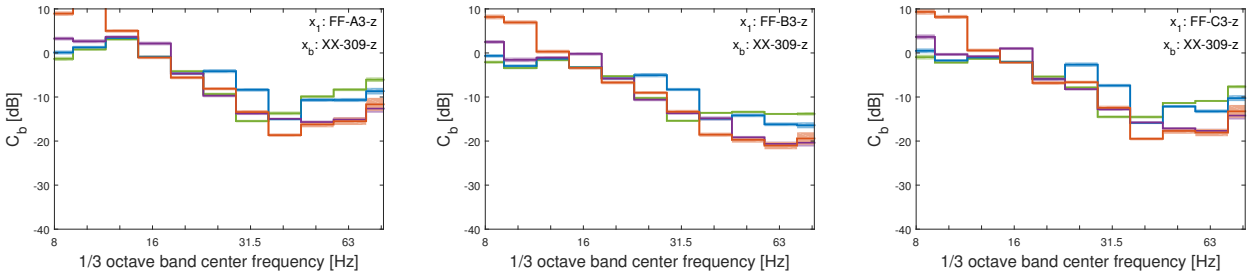

(d)

Figure 10: Coupling loss values calculated with receiver points $\mathbf{x}_b$ at various floors with locations (a) XX-125-z; (b) XX-113-z; (c) XX-101-z; and (d) XX-309-z, determined using the passage of 117 passenger train passages (77-100 km/h). Free field receiver points $\mathbf{x}_1$ are located 1 m from the building on measurement lines A, B and C (left to right). Shaded areas indicate the 95% confidence intervals.

ACKNOWLEDGEMENTS

The first author is a postdoctoral fellow of the Research Foundation Flanders (FWO). The second author is a postdoctoral fellow of KU Leuven. The third author is a PhD student supported by the FWO. The support of these funders is gratefully acknowledged. The field measurement study presented in this paper was conducted as part of the project OT/13/059 “Quantifying and reducing uncertainty in structural dynamics” funded by the Research Council of KU Leuven. These measurements were performed in part by Manthos Papadopoulos, Jie Zhang, and Avisek Mukherjee of the Department of Civil Engineering of KU Leuven.

REFERENCES

Bovey, E.C. 1983. “Development of an impact method to determine the vibration transfer characteristics of railway installations.” 87 (2): 357–370.

Deutsches Institut für Normung. 1995. *DIN 45672 Teil 2: Schwingungsmessungen in der Umgebung von Schienenverkehrswegen: Auswerteverfahren.* Deutsches Institut für Normung.

Hanson, C.E., D.A. Towers, and L.D. Meister. 2005. *High-speed ground transportation noise and vibration impact assessment.* HMMH Report 293630-4. U.S. Department of Transportation, Federal Railroad Administration, Office of Railroad Development, October.

———. 2006. *Transit noise and vibration impact assessment.* Report FTA-VA-90-1003-06. U.S. Department of Transportation, Federal Transit Administration, Office of Planning and Environment, May.

Hood, R.A., R.J. Greer, M. Breslin, and P.R. Williams. 1996. “The calculation and assessment of ground-borne noise and perceptible vibration from trains in tunnels.” 193:215–225.

International Organization for Standardization. 2005. *ISO 14837-1:2005 Mechanical vibration - Ground-borne noise and vibration arising from rail systems - Part 1: General guidance.* International Organization for Standardization.

Kuo, K.A., G. Lombaert, and G. Degrande. 2016. “Quantifying uncertainties in measurements of railway vibration,” 62–69. Proceedings of the 12th International Workshop on Railway Noise IWRN12. Terrigal, Australia, September.

———. 2017. “Quantifying dynamic soil-structure interation for railway-induced vibrations.” Proceedings of the 10th European Conference on Structural Dynamics: Eurodyn 2017. Rome, Italy, September.

Kuppelwieser, H., and A. Ziegler. 1996. “A tool for predicting vibration and structure-borne noise immissions caused by railways.” 193:261–267.

Madshus, C., B. Bessason, and L. Hårvik. 1996. “Prediction model for low frequency vibration from high speed railways on soft ground.” 193 (1): 195–203.

Nelson, J.T., and H.J. Saurenman. 1987. “A Prediction Procedure for Rail Transportation Groundborne Noise and Vibration.” 1143:26–35.

Xia, H., J.G. Chen, P.B. Wei, C.Y. Xia, G. De Roeck, and G. Degrande. 2009. “Experimental investigation of railway train-induced vibrations of surrounding ground and a nearby multi-story building.” *Earthquake Engineering and Engineering Vibration* 8 (1): 137–148. http://dx.doi.org/10.1007/s11803-009-8101-0.